PERGAMON

International Journal of Solids and Structures 39 (2002) 4999–5012

INTERNATIONAL JOURNAL OF SOLIDS and STRUCTURES

www.elsevier.com/locate/ijsolstr

Influence of imperfections on the performance of metal foam core sandwich panels

H. Bart-Smith [a,*], J.W. Hutchinson [b], N.A. Fleck [c], A.G. Evans [d]

[a] *Department of Mechanical and Aerospace Engineering, University of Virginia, Charlottesville, VA 22904, USA*
[b] *Division of Engineering and Applied Science, Harvard University, Cambridge, MA 02138, USA*
[c] *Department of Engineering, University of Cambridge, Cambridge, CB2 1PZ, UK*
[d] *Mechanical & Environmental Engineering, University of California, Santa Barbara, CA 93106, USA*

Received 26 September 2001

Abstract

Sandwich panels and beams are used in bending and compression dominated components. The retention of their load capacity in the presence of imperfections is a central consideration. To address this issue, sandwich beams with metallic foam cores have been tested in four-point bending following the introduction of imperfections, created by impressing the face sheets. Limit load expressions for face yielding, core shear, and indentation failure have been developed and used to construct failure mechanism maps. From these maps, specimen designs were determined. Imperfections were introduced by indenting to varying penetrations. The indents were located on both the compressive and tensile side of bending configurations. Experimental measurements of the load/deflection response are obtained and compared with finite element results.

Keywords: Sandwich panels; Metallic foams; Mechanism maps; Four-point bending

1. Introduction

Before ultra-light sandwich structures based on metal foam cores can be realistically considered for use in structural applications (Ashby et al., 2000), some measure of their ability to retain load capacity in the presence of imperfections must be examined and quantified. For example, structural integrity after locally impressing the core needs to be understood. Previous work on sandwich beams and panels has established a mechanism map approach, based on limit loads, to establish the load capacity (Ashby et al., 2000; Chen et al., 2001; Bart-Smith et al., 2001; McCormick et al., 2000). It has also been demonstrated that implementation of a constitutive model for the core material captures the main deformation features witnessed in experiments (Ashby et al., 2000; Bart-Smith et al., 2001; Deshpande and Fleck, 2000). With this background, a simulation and measurement protocol for addressing the influence of imperfections is developed.

* Corresponding author. Tel.: +1-434-924-0701; fax: +1-434-924-0701.
E-mail address: hilary@virginia.edu (H. Bart-Smith).

0020-7683/02/$ - see front matter
PII: S0020-7683(02)00250-0

Table 1
Material properties

(i) Face sheet materials Aluminum alloy	Young's modulus E_f (GPa)	Yield strength σ_Y (MPa)
6061-T6	69	268
Nominal 6061-T0	69	40
Half hardened	69	100
(ii) ALPORAS core material (Akiyama et al., 1987; Sugimura et al., 1997)		
Relative density	0.08	
Young's modulus, E_C^{unload} (MPa)	230	
Shear modulus, G_C (MPa)	90	
Yield strength, σ_c (MPa)	1.5	
Plastic Poisson ratio, v^P	0	
Elastic Poisson ratio, v	0.3	
Yield coefficient, β	$3\sqrt{2}$	

Four-point bending is chosen as the testing method. Impressions are used to simulate imperfections that might arise in real applications. Mechanism maps are constructed from limit load expressions for the dominant failure modes: face yield, core shear, and indentation (Ashby et al., 2000). Imperfections are expected to affect the stiffness and limit load when either face yield or core shear are the operative failure modes. Accordingly, specimens are designed to fail by one of these mechanisms. By measuring the load–displacement responses on impressed panels, and comparing with those for "pristine" panels, the extent of the degradation in stiffness and limit load will be explored. The panels consist of a closed cell Al alloy foam core (trade name Alporas, Akiyama et al., 1987; Sugimura et al., 1997) and several different Al alloy faces with varying yield strength. These experimental results are compared with numerically generated load–displacement curves, based on the material properties summarized on Table 1.

2. Philosophy

Given that the impressions reduce the section thickness, as well as compress the core and stretch the face sheets, failure by face yield and core shear are the mechanisms most likely to be affected (Ashby et al., 2000). Assessment of the degradation requires that limit loads be determined and failure maps constructed. To determine the relevant loads, prior results (Chen et al., 2001; Bart-Smith et al., 2001) have been modified to take into account the flat platen fixtures used in this study. The main geometric parameters for the beam of width b are defined in Fig. 1.

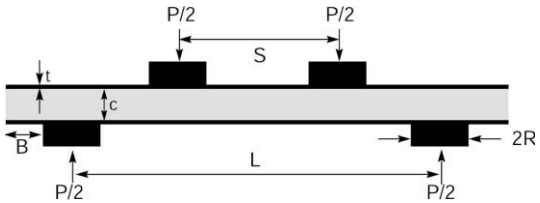

Fig. 1. Four-point bend configuration used to probe experimentally the effects of damage on the load–displacement response and failure mechanism.

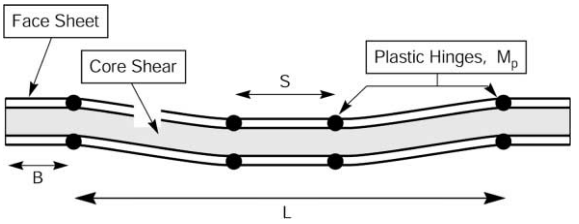

Fig. 2. Schematic of kinematically admissible displacement field (no shear in overhang) for failure by core shear.

The limit load expressions are as follows: for face yield (neglecting the minimal effects of the core),

$$\frac{P_{\mathrm{FY}}}{\sigma_{\mathrm{c}} bL} \equiv 4\frac{c+t}{L-S}\frac{t}{L}\frac{\sigma_{\mathrm{Y}}}{\sigma_{\mathrm{c}}} \tag{1}$$

for indentation,

$$\frac{P_{\mathrm{I}}}{\sigma_{\mathrm{c}} bL} \equiv 4\frac{t}{L}\sqrt{\frac{\sigma_{\mathrm{Y}}}{\sigma_{\mathrm{c}}}} + 4\frac{R}{L} \tag{2}$$

and for core shear, absent shear deformation in the overhang (Fig. 2),

$$\frac{P_{\mathrm{CS}}}{\sigma_{\mathrm{c}} bL} \equiv 4\frac{t}{L}\frac{t}{L-S}\frac{\sigma_{\mathrm{Y}}}{\sigma_{\mathrm{c}}} + 2\frac{c}{L}\frac{\tau_{\mathrm{c}}}{\sigma_{\mathrm{c}}} \tag{3}$$

The corresponding compliance is given by (Allen, 1969; Gibson and Ashby, 1997):

$$C \equiv \frac{\delta}{P} = \frac{2(L-S)^3}{B_1 E_{\mathrm{f}} btc^2} + \frac{L-S}{B_2 G_{\mathrm{C}} bc} \tag{4}$$

where $B_1 = 48$ and $B_2 = 4$. In these formulae, c is the core thickness, t the face thickness, b the beam width, S the spacing between the inner platens used in the bend test and L the span. The quantities σ_{c}, τ_{c} and G_{C} refer to the compressive and shear strengths of the core, and its shear modulus, respectively. The quantity σ_{Y} is the yield strength and E_{f} the Young's modulus for the faces. The total load is given by P, with the subscripts FY, I and CS, designating face yield, indentation and core shear, respectively.

In most of the following examples, a relative inner span width, $S/L = 0.45$, and platen width, $R/L = 0.05$, are used. Based on the properties of 6061-T6 ($\sigma_{\mathrm{Y}} = 268$ MPa) face sheets and the Alporas core materials (Table 1), the failure map in Fig. 3a was constructed, with c/L and t/L as coordinates. A map has also been constructed for a face material having nominal yield strength $\sigma_{\mathrm{Y}} = 40$ MPa (Fig. 3b). For the former, with strong faces, core shear is the dominant mode of failure, in accordance with (3). In such cases, the load capacity should not be strongly affected by imperfections located between the inner platens, which experience bending (no shear). A greater effect of imperfection is anticipated with the softer faces, which fail by face yield, expressed by (1). The face material used for the experimental measurements (6061-T6) had a higher than expected yield strength ($\sigma_{\mathrm{Y}} = 100$ MPa), such that the test dimensions were at the transition between face yield and core shear, as elaborated below. In order for face yielding to be the operative mode of failure $S/L = 0.18$ and $R/L = 0.035$.

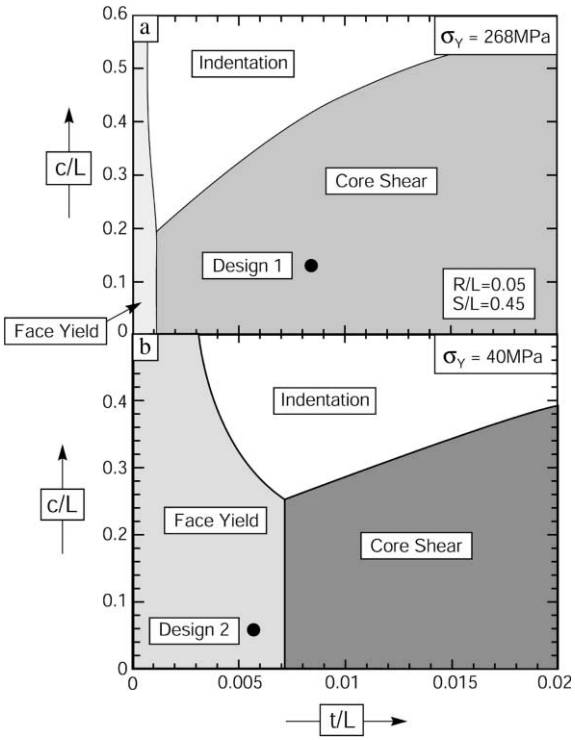

Fig. 3. Mechanism maps showing failure domains: (a) map for sandwich panels with Alporas core and Al alloy 6061-T6 faces, (b) map for same core with soft (6061-0) faces. Table 2 gives dimensions for specimens.

Table 2
Specimen dimensions

Design	Face	Core	t/L	c/L	t (mm)	c (mm)	L (mm)	$2R$ (mm)	S (mm)
1	6061-T6	Alporas	0.01	0.125	0.8	10	80	8	36
2	6061-0	Alporas	0.005	0.063	0.8	10	160	16	72
3	HH	Alporas	0.036	0.045	0.8	10	224	16	40

3. Measurements

3.1. Procedure

The measurement procedure was as follows. An impression, width $2R$, was introduced at the center of the specimen. To achieve this, a flat platen, similar in design to the loading platens, was bonded to the top surface at the midpoint of the specimen (Fig. 4). The bottom surface was bonded to a compression plate. Using a servo-hydraulic system, the specimens were placed between compression fixtures and indented by δ_{indent} at 0.3 mm/min. Loads and displacements were recorded. After impressing, the beams were placed in four-point bending, with the impressed side subject to either tension or compression. For this purpose, flat platens made from high strength steel were used. Again, loads and displacements were recorded. A strain gauge was placed on the tensile side of pristine beams to examine the deformation of the face sheet, allowing verification of the dominant mode of failure.

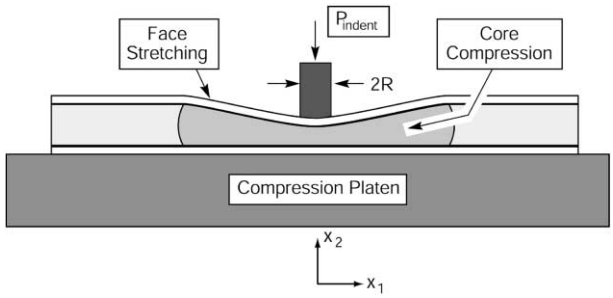

Fig. 4. Schematic showing indentation of sandwich beam.

3.2. Results

The load–displacement curve measured upon indentation of the panel with the strong faces (6061-T6) is summarized on Fig. 5. Flexural measurements obtained on the core shear design for panels with strong (6061-T6) faces containing imperfections up to 3 mm deep, gave the load–displacement curves presented on Fig. 6. Optical images of the core between the inner and outer loading points affirmed that core shear was the dominant failure mode (Fig. 7a). The maximum load and the stiffness measured in each test are summarized on Table 3. Note that, in most cases, the limit loads are essentially unaffected by the imperfections: whereas the stiffness is slightly reduced as the imperfection depth increases. Tests with 3 mm imperfections on the tensile surface were the exception (Fig. 6a). In such cases, the stiffness was markedly lower, because the face sheets debonded in the region where the indent was introduced (Fig. 7b). Despite this stiffness degradation, the loads recovered to levels almost the same as those for the pristine beam.

The corresponding load–displacement response for beams with soft faces ($\sigma_Y = 100$ MPa) highlight the greater sensitivity of the load capacity to imperfections when failure occurs by face yielding (Fig. 8a). When on the tensile side, a 3 mm impression reduces the peak load to about 2/3 that achieved with pristine beams. Also, as in the case for core shear failure, the imperfection causes a marked reduction in the stiffness. Images taken during the test (Fig. 8b) indicate that, in this case, the face remains attached to the core (no

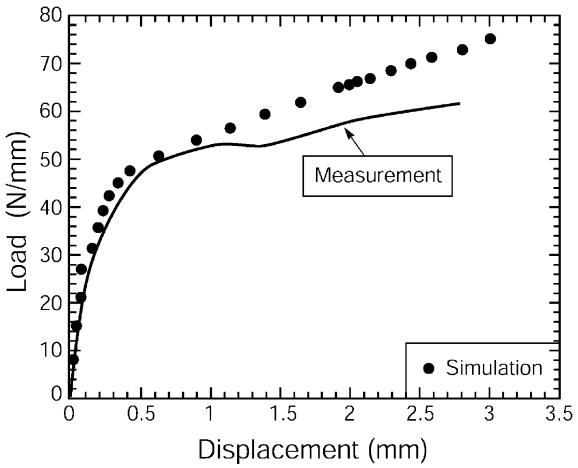

Fig. 5. Measured and simulated load–deflection curves during indentation (Bart-Smith et al., 2001) of a panel with strong faces. The results are essentially the same for the soft faces since the force is dominated by the compression of the core.

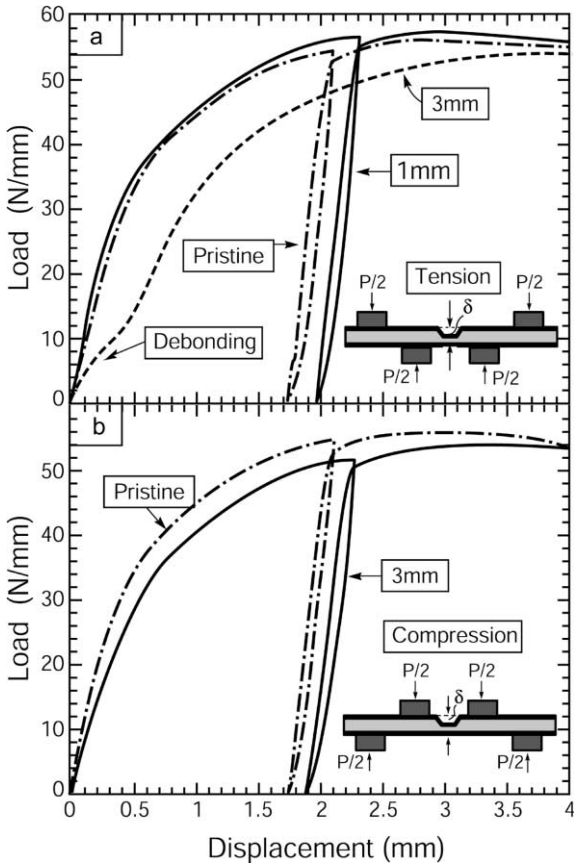

Fig. 6. Load–deflection curves measured in flexure for a panel with strong face sheets (6061-T6): (a) indent on tensile side; (b) indent on compressive side. Note that in (a), for the case with a 3 mm impression, the face debonded upon loading.

debonding). Instead, the face sheet stretches and ''pulls back'' the indented core, simultaneously deforming the top face.

4. Simulations

4.1. Method

The commercial finite element code, ABAQUS, was used to simulate the deformation. A user-defined subroutine for metallic foams, after Deshpande and Fleck (2000), was implemented, with the stress/strain response measured on bulk foam used to describe the core material. The finite element mesh, comprising half of the specimen, uses 8-noded plane strain elements. The analysis was separated into three steps: (i) to simulate indentation, displacement boundary conditions were prescribed at nodes connected to the platen, while the bottom surface nodes were fixed in the one- and two-directions as defined in Fig. 4; (ii) after indentation, the loads over all nodes were reduced to zero; (iii) to simulate bending, with free rotation of the platens, a displacement boundary condition was applied to the center node at the inner load platen, with multi-point constraints applied over all other contact nodes (Bart-Smith et al., 2001).

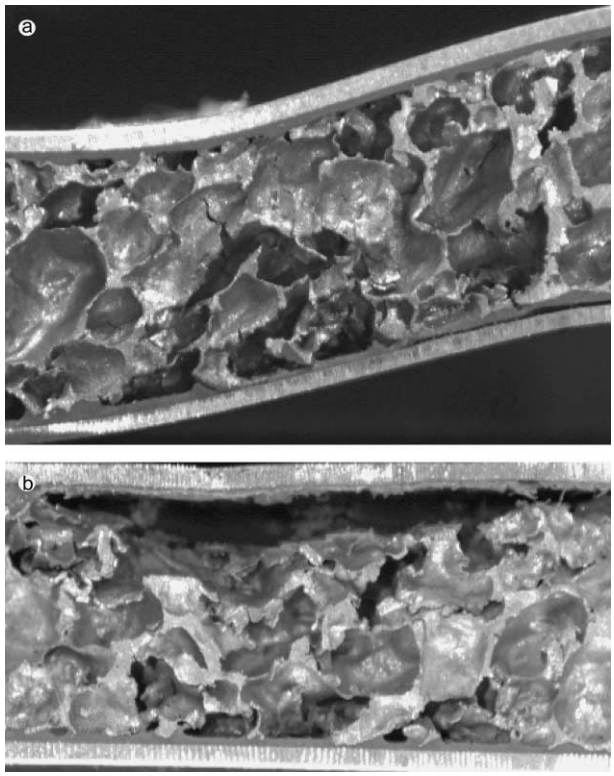

Fig. 7. Optical image showing (a) core shear deformation, (b) face sheet debonding for a test with a 3 mm indent on the tensile side (see Fig. 6a).

Table 3
Experimental results

Design	δ_{indent} (mm)	Maximum load (kN/m)	Stiffness (MN/m^2)	
			Initial	Unloading
Tension	0	56	100	232
	1	57	80	227
	3	54	_[a]	_[b]
Compression	0	56	100	235
	1	54	67	235
	3	54	69	211

[a] The stiffness cannot be calculated due to debonding.
[b] Unloading was not performed due to debonding.

4.2. Load–displacement curves

The simulated indentation response, shown on Fig. 5, is consistent with the experimental measurements, as shown previously (Ashby et al., 2000; Chen et al., 2001; Bart-Smith et al., 2001; McCormick et al., 2000).

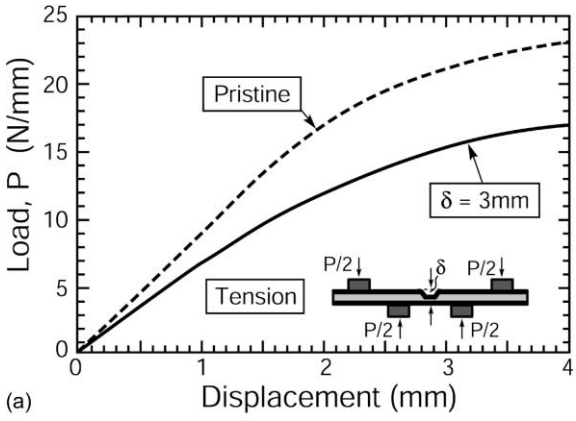

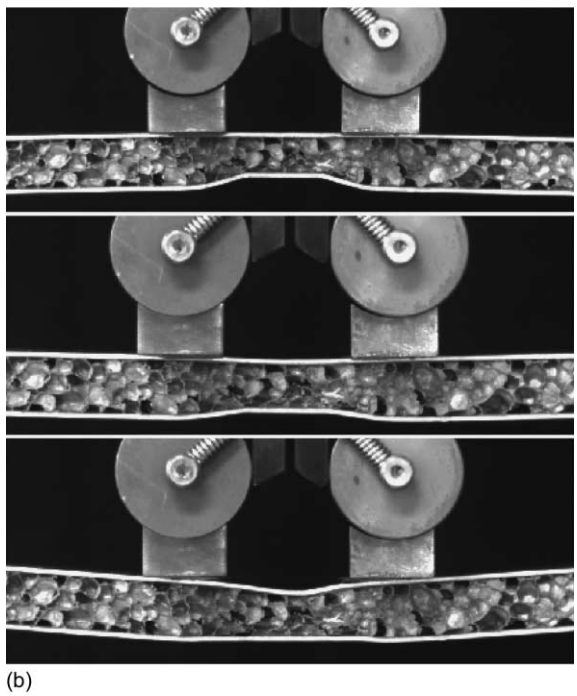

Fig. 8. (a) Load–deflection curve measured in flexure for a panel with soft face sheets (half hardened aluminum) with indent on tensile side. (b) Optical images showing the influence of face sheet stretching on the indented core.

The simulated curves for bending are presented on Figs. 9 and 10. For panels with strong faces that fail by core shear (Fig. 9), impressions up to 3 mm deep have minimal effect on the load/deflection response when the imperfections are on the *compressive side* (Fig. 9a). Only at $\delta_{\text{indent}} = 5$ mm (half the core thickness) is there a diminution in load capacity, by about 20%. When the indent is on the *tensile side* of the beam, the load capacity diminishes more systematically as the indentation depth increases (Fig. 9b). But still, the effects are small. Impressions with depth, $\delta_{\text{indent}} = 3$ mm, reduce the load capacity by only 10%. A more detailed analysis reveals that small impressions, $\delta_{\text{indent}} \leqslant 2$ mm, when on the compressive side, *slightly elevate* the load capacity relative to pristine beams (Fig. 9a). The origins of this effect are addressed below.

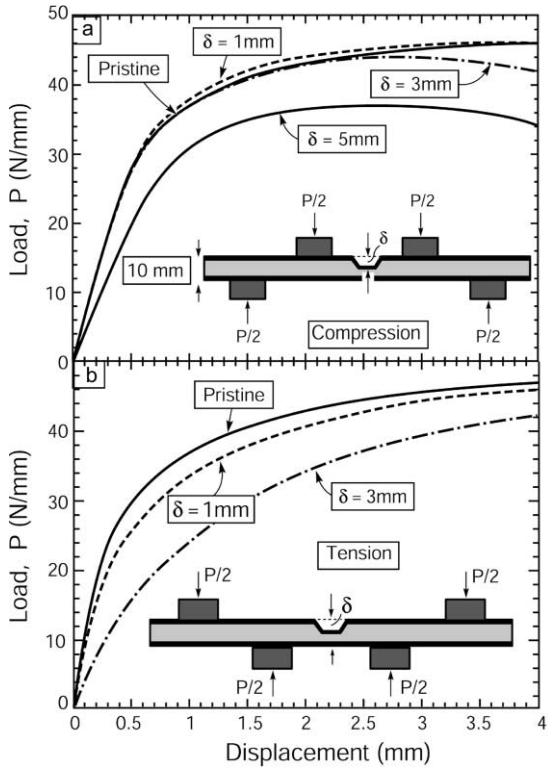

Fig. 9. Characteristic load–deflection curves calculated by finite elements for the core shear design. (a) Indent on compressive side and (b) indent on tensile side. Each scenario is compared with the pristine panel response.

For the beams that fail by face yield (where $\sigma_Y = 40$ MPa), the response is much more sensitive to the presence of imperfections (Fig. 10a and b). There is a systematic diminution in the load capacity once the impressions are in the size range, $\delta_{indent} \geqslant 1$ mm. Moreover, the softening beyond the peak load now proceeds quite rapidly. As before, the load degradation at larger impression depths is greater when the impression is on the tensile (rather than the compressive) side of the beam. Notably, for impressions, $\delta_{indent} = 3$ mm, the load maximum decreases to about 1/3 that for the pristine beam (Fig. 10b). Note that, again, small imperfections ($\delta_{indent} = 1$ mm) on the compressive side slightly elevate the load capacity relative to the pristine beams (Fig. 10a). The simulations of the test with faces having yield strength $\sigma_Y = 100$ MPa (Fig. 10c) reveal a response essentially identical to the experiments (Fig. 8a). The diminishing effect of the imperfection on the load capacity, relative to $\sigma_Y = 40$ MPa, is a consequence of the role of core shear in the test. That is, by testing at the boundaries between mechanisms, the degradation caused by imperfections is reduced.

Typical stiffness results are plotted on Fig. 11 for the example of a panel with strong faces containing impressions, $\delta_{indent} = 5$ mm. It is apparent that, since the incremental stiffness begins to diminish as soon as the displacement is imposed, the panel does not have a true elastic domain. The role of residual stress in the core (after indentation) in governing this response is explored below. In principle, unloading could have assessed the influence of the impressions on the actual stiffness, but this was not pursued. Nevertheless, note that the incremental stiffness extrapolated to zero displacement is lower than that for the pristine beam by 15–20%.

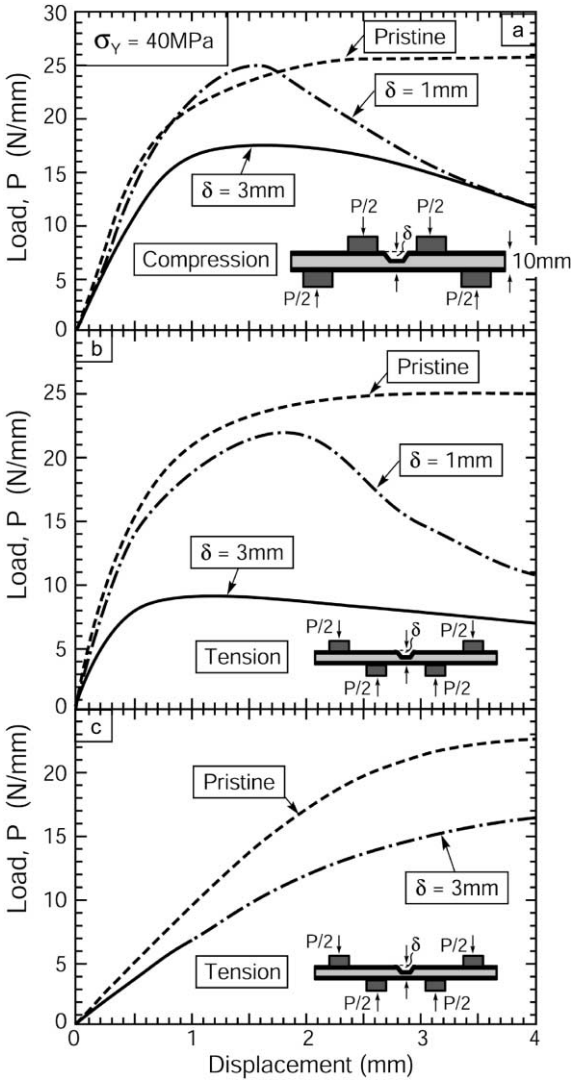

Fig. 10. Characteristic load–deflection curves calculated by finite elements for face yield design. (a) Indent on compressive side, (b) indent on tensile side and (c) each scenario is compared with pristine panel response.

Cursory comparison of these calculated results (Figs. 9 and 10) with the measured curves (Figs. 6 and 8) reveals that the simulated limit loads are somewhat lower (by about 20%). This discrepancy is attributed to the effect of core thinness on its shear strength, elucidated in earlier studies (Chen et al., 2001; Bart-Smith et al., 2001; McCormick et al., 2000). While this effect has not been included in the present numerical assessment, it is not expected to change the trends elucidated in the simulations: only the absolute values will differ.

4.3. Stress distributions

Some of the effects of impressions on the load–displacement responses noted above are attributed to residual stresses generated by indentation. These stresses are explored in this section. Indentation crushes

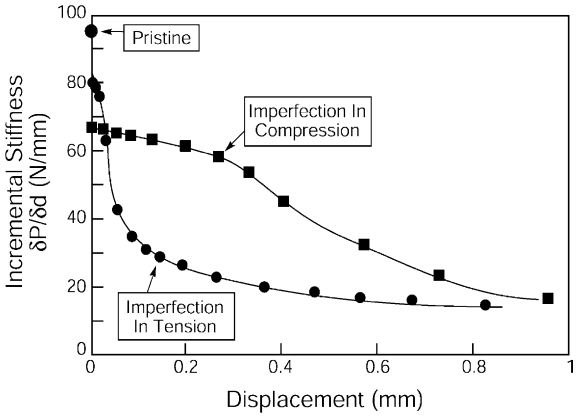

Fig. 11. The incremental stiffness calculated for panels with strong faces containing imperfections with $\delta_{\text{indent}} = 5$ mm on the tensile and compressive sides of the panel. The stiffness for the pristine beam is also indicated.

the core locally and stretches the face sheet, generating tensile stresses in the face that exceed yield near the indent corners (Fig. 12a, Bart-Smith et al., 2001), and resulting in residual stresses upon unloading (Fig. 12b). Locally, near the corners, these residual stresses are at the yield strength of the face material

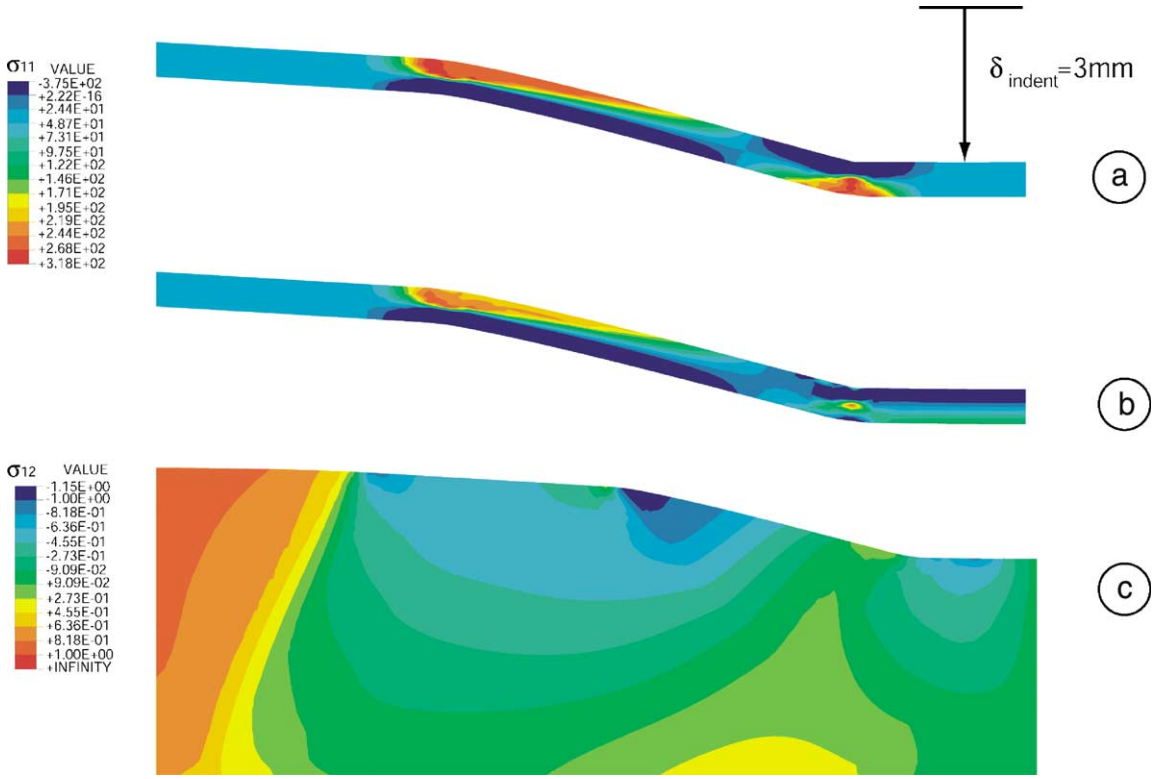

Fig. 12. The stresses induced upon indentation of a panel with strong faces to a depth, $\delta_{\text{indent}} = 3$ mm. (a) The stresses σ_{11} in the face upon impressing, (b) the residual stresses σ_{11} in the face and (c) the residual stresses σ_{12} in the core.

(Fig. 12b), even for small impressions. These are the stresses that have a substantive effect on the displacement response upon subsequent loading, as elaborated below. Shear stresses exceeding the yield strength generated in the core during indentation remain upon unloading (Fig. 12c). These residual stresses extend laterally by several multiples of the core thickness. Accordingly, they extend beyond the position of the inner load platens used for the subsequent bending tests. The consequence is the onset of core yielding immediately upon load application in bending, resulting in the "soft" incremental stiffness evident on Fig. 11.

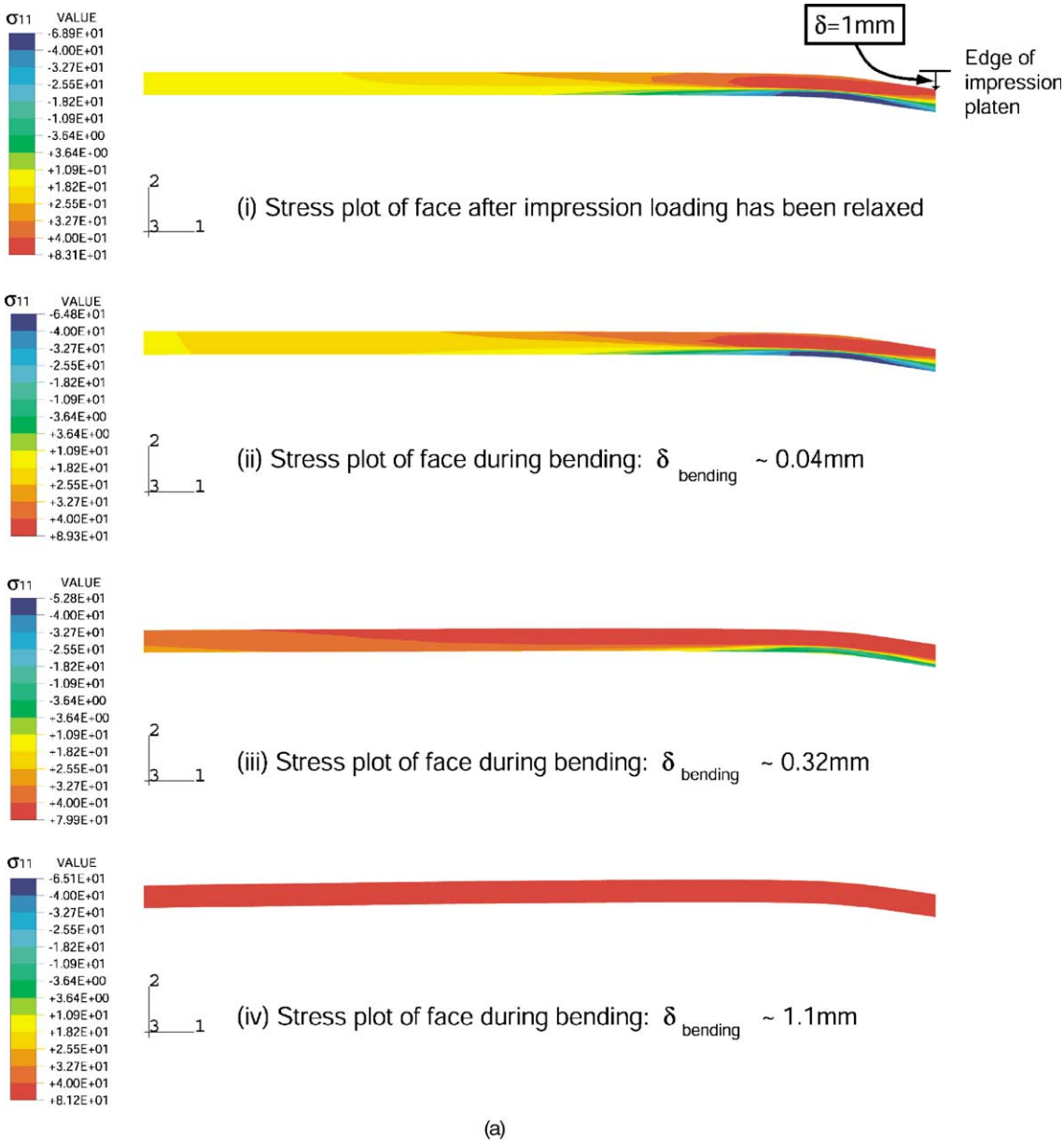

Fig. 13. The evolution of the stresses σ_{11} in the impressed face upon bending. The results are for a panel with strong faces with an impression, $\delta_{\text{indent}} = 1$ mm: (a) impression on tensile side and (b) on compressive side.

Upon bending, the response of the faces differs depending on whether the imperfection is on the *tensile* or *compressive* side. On the tensile side, plots of the evolution of the axial (σ_{11}) stress with bending displacement, δ_{bending} (Fig. 13a) reveal that the plastic zone around the imperfection begins to expand immediately upon applying the displacement and grows systematically as the displacement increases. The associated strains adversely affect the limit loads, as demonstrated on Figs. 9 and 10 and further discussed below. Conversely, when the indent is on the compressive side, as the bending displacements are imposed (Fig. 13b), the *residual plastic zone shrinks* as the compression unloads the faces. This zone shrinkage is the

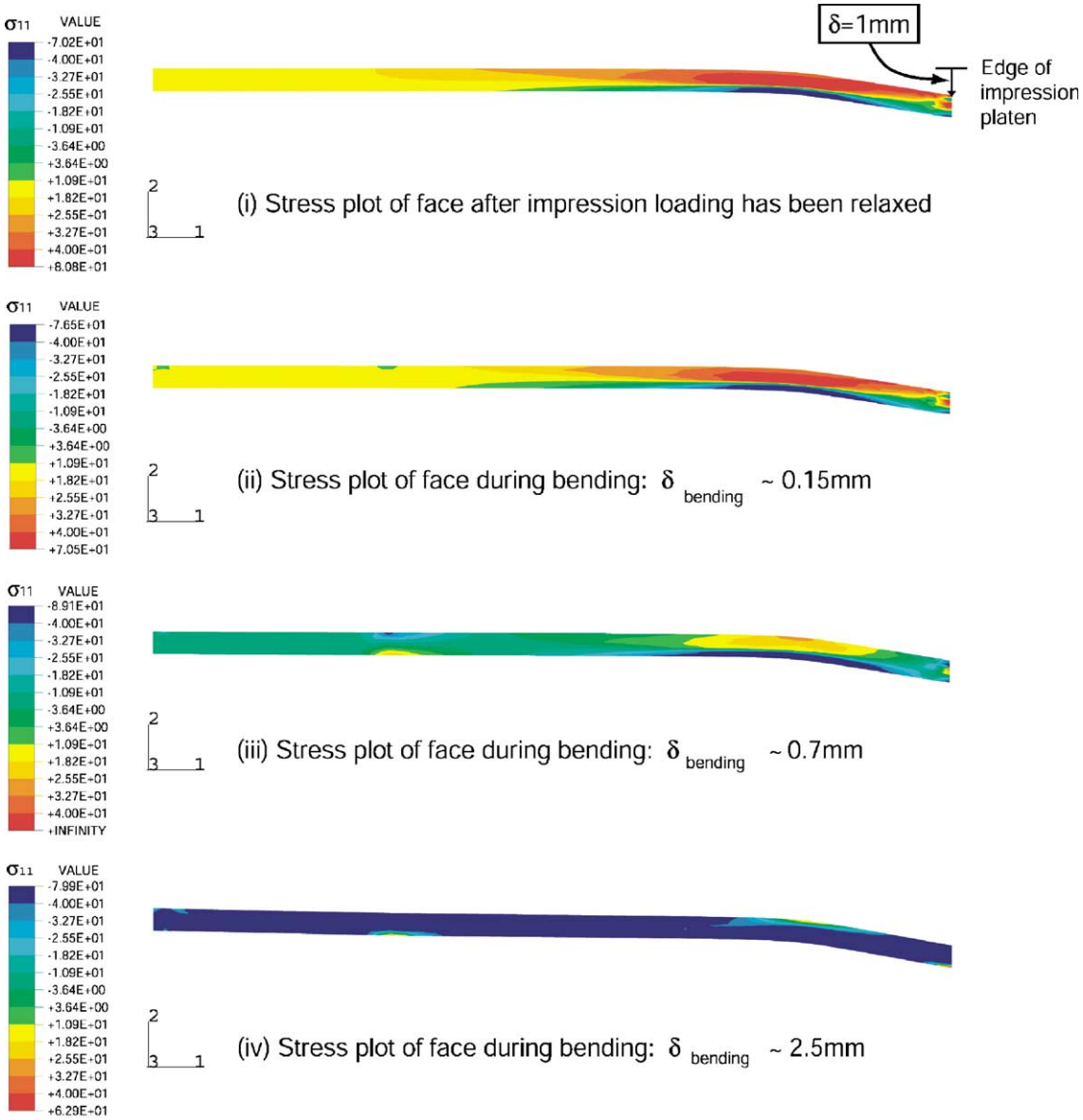

(b)

Fig. 13 (*continued*)

origin of the larger load capacity upon initial loading (relative to pristine beams) found for small impressions (Figs. 9 and 10).

5. Concluding assessment

The experimental measurements and the numerical simulations of the effects of imperfections on the load capacity and stiffness of foam core panels are broadly consistent (c.f. Figs. 6 and 8 with Figs. 9 and 10), giving confidence in the use of simulations to probe a range of other potential imperfection responses. That is, the detailed effects of impressions on the load/deflection response of panels with both strong and soft faces are captured, quite accurately, by the numerical simulations. The one substantive difference arises for larger impression located on the tensile side. The experiments reveal that the face within the imperfection debonds, causing an appreciable diminution in stiffness. The simulations do not reflect the influence of this failure mechanism, because a fracture criterion has not been included in the finite element model. The numerically generated loads are also somewhat lower than those measured experimentally. The disparity is understood (Bart-Smith et al., 2001). It is associated with the influence of core thinness on the core shear strength: an effect that can be incorporated into future simulations.

Finally, it is noted that the analytical formulae (Eqs. (1)–(4)) do not incorporate the phenomena needed to discern the effects of the impressions on either the limit loads or the stiffness. One major limitation is that the formulae do not account for the residual stresses (Figs. 12 and 13), which affect the nominal compliance as well as the effective yield strengths of the faces and the core, as discussed above.

References

Ashby, M.F., Evans, A.G., Fleck, N.A., Gibson, L.G., Hutchinson, J.W., Wadley, H.G.N., 2000. Metal Foams: A Design Guide. Butterworth Heinemann.

Chen, C., Harte, A.M., Fleck, N.A., 2001. The plastic collapse of sandwich beams with a metallic foam core. Int. J. Mech. Sci. 43, 1483–1506.

Bart-Smith, H., Hutchinson, J.W., Evans, A.G., 2001. Measurement and analysis of the structural performance of cellular metal sandwich construction. Int. J. Mech. Sci. 43, 1945–1963.

McCormick, T.M., Miller, R., Kesler, O., Gibson, L.J., 2000. Failure of sandwich beams with metallic foam cores. Int. J. Solids Struct. 38, 4901–4920.

Deshpande, V.S., Fleck, N.A., 2000. Isotropic constitutive models for metallic foams. J. Mech. Phys. Solids 48 (6), 1253–1283.

Akiyama, S., Imagawa, K., Kitahara, A.A., Nagata, S., Morimoto, K., Nishikawa, T., 1987. US Patent 4, 713, 277, 15 December.

Sugimura, Y., Meyer, J., He, M.Y., Bart-Smith, H., Grenestedt, J., Evans, A.G., 1997. Acta Mater. 45 (12), 5245–5259.

Allen, H.G., 1969. Analysis and Design of Structural Sandwich Panels. Pergamon.

Gibson, L.G., Ashby, M.F., 1997. Cellular Solids. Cambridge University Press.